CHAPTER 3

# *Mass Transport Across Atomically Thin Membranes*

K.-P. SCHLICHTING AND H. G. PARK*

Nanoscience for Energy Technology and Sustainability, Department of Mechanical and Process Engineering, Eidgenössische Technische Hochschule (ETH) Zürich, Tannenstrasse 3, Zürich CH-8092, Switzerland
*Email: parkh@ethz.ch

## 3.1 Introduction

Membrane separation technology is drawing growing attention today in research and technology due to its promise of process intensification toward resource saving and process simplicity.[1] The simplicity stems from the nature of a separation membrane, a barrier that allows disproportionate transport of one species over the other. Chemical separation results from this transport disproportionation. Membrane-based separation can consume far less energy and resources than other separation technologies do based on an energy intensive phase change (*e.g.* cryogenic distillation in gas separation or thermal distillation in water treatment).[2,3] Despite this promise, the widespread economic use of membranes in separation applications has not been seen yet, which is ascribable to limits in material properties, challenges of upscaling, and issues of economic fabrication. One of the overarching research goals of membrane-based separation technology is the establishment of enhanced membrane performance to exploit the technological and economic potential and to promote the engineering efforts toward membrane upscaling and cost-effective process optimization.

Nanoscience & Nanotechnology Series No. 47
Graphene-based Membranes for Mass Transport Applications
Edited by Pengzhan Sun and Hongwei Zhu

Published by the Royal Society of Chemistry, www.rsc.org

Separation membranes can be largely classified into two categories: dense membranes, *i.e.*, membranes not possessing definable porous structures, whose transport mechanism is conveniently described by the solution-diffusion model; and porous membranes, for which the hydrodynamic and sub-continuum transport models are often utilized.[2,4] To describe the separation performance of a membrane, its permeance – the transport rate per unit area normalized by a driving force – and selectivity – the permeance ratio of the species of interest – comprise the main figures of merit. In general, the permeance of a membrane material is inversely proportional to its thickness, since friction forces with pore walls or diffusion pathways decrease by shortening the effective transport lengths. This inverse relationship leads to the desire of making ever thinner membranes to enhance the performance. Selectivity of dense membranes, on the other hand, depends typically on the solubility and diffusion ratios of the permeating species and is therefore an intrinsic property of the membrane material. Contrary to dense membranes, porous membranes separate on the basis of molecule–pore interactions, related to the ratio between pore size and molecular length scale. This interaction of porous membranes allows the selective transport behaviour in principle to be decoupled from the intrinsic material properties, potentially offering flexibility in the determination of their selectivity. The thickness of porous membranes contributes to the permeance by controlling the entire amount of the molecule–pore friction mechanism.

For a given pore size, the membrane thickness can be decreased all the way down to an atomic dimension that graphene and 2D materials can offer. At the atomic dimension of membrane thickness, it is expected that the friction and viscous interaction of transporting fluid in the pore interior disappear or are minimized to permit very rapid permeation. In fact, in the limit of vanishing thickness, the transport pathway is supposed to cause a singularity in the transport rate based on continuum model prediction. However, as shall be discussed later in this text, pores formed on graphene can help avoid the Fickian singularity in a way that omission of conventional determinants of transport physics brings about the emergence of other transport-governing phenomena related to the 3D-to-2D transition. Ultimately, in the limit of the 2D material thickness, the lattice spacing of 2D crystals can be considered similar to the free volume in dense membranes such that it raises a question of whether a description of 2D membranes by a generalized solution diffusion mechanism may work out. For this reason, it is important to study the transport physics across 2D membranes because conventional models may not be able to accurately describe mass transport across graphene membranes.

A prerequisite question to answer prior to the utilization of graphene as a porous membrane is whether it is permeable in its pristine form to the species it should separate. In 2008, Bunch and co-workers performed experiments to answer this question.[5] They pressurized a micrometre-sized cavity in $SiO_2$ covered by mechanically exfoliated graphene flakes and

subsequently measured the deflection of the bulging graphene with an atomic force microscope. For various gases including He, they could show that the deflection over time of the pressurized graphene blister is independent of the layers of graphene (up to 75 layers were tested) and simultaneously matches the diffusion rate through their substrate. Further analysis of a tunnelling probability across pristine graphene revealed that pristine graphene is impermeable to gases as small as He and may pose a formidable barrier to mass transport. Consequently, in its pristine form, graphene is not directly suited as a separation membrane unless pores are introduced into its structure. Pore formation has been immediately demonstrated experimentally *via* energetic electron beam irradiation,[6] energetic ion beam bombardment,[7] heterogeneous oxidation through plasma[8] or harsh chemistry.[9] Notably, the pores created in these ways remain stable for an intermediate-to-long period of time, shedding light on the feasibility of porous graphene for membrane applications.

## 3.2 Gas Transport Across Porous Graphene Membranes

The study of gas transport across porous graphene membranes has been motivated by graphene's potential impermeability to gases despite the atomic thinness. Once the graphene is chopped open to bear tiny pores, the thinness of graphene in turn acts as an ultimate gas permeator. In this light, the focus of gas transport study across porous graphene has been geared toward engineering highly selective membrane materials. High selectivity is expected for pores that are of similar size to the kinetic diameters of the gas molecules to be separated, a mechanism known as molecular sieving.

The pioneers of gas separation applications of porous graphene are Jiang and co-workers, who have used density functional theory (DFT) to investigate the transport behaviour of light inorganic gases through subnanometre pores on graphene.[10] After removing two hexagonal carbon rings (10 carbon atoms) from a graphene lattice in a modelling domain, they considered two types of pores: one by hydrogen passivation of all the carbon dangling bonds, and the other by nitrogen and hydrogen passivation. Such passivation constricted the pore width from 3.0 Å to 2.5 Å on the basis of the isoelectric surface of the electron density distribution of the pore edge atoms (0.02 e/Å$^3$). Ballistic transport of $H_2$ and $CH_4$ across these model pores undergoes diffusion barriers describable with activation energies of an Arrhenius formula (assuming an identical exponential prefactor). Once determining the smallest width of a pore to dictate the permeance, they found out that molecules orient preferentially against the pore edges during the passage and that this orientation is reliant on the molecule and edge-passivation pair. The $H_2/CH_4$ selectivity has been reported to be as high as $10^8$ for the 3.0 Å pore and $10^{23}$ for the smaller pore. They attributed the 15-order-of-magnitude rise in the selectivity to the exponential dependence

of the gas diffusion barrier, elevating greatly when the constricting width becomes commensurable with the kinetic diameters of the transporting molecules (2.89 Å for $H_2$ and 3.80 Å for $CH_4$). Even though they have not extended the modelling beyond the ballistic transport for simplicity, this study has predicted the potentially astounding selectivity of graphene membranes for gas separation and proposed an activation energy of pore passage as an indicator of the cross-graphene-pore gas transport.

Following this pioneering work, Li *et al.* investigated the permeation of $H_2$, CO, $CO_2$, and $CH_4$ with DFT by considering a graphene pore as large as one benzene-ring size passivated by hydrogen atoms.[11] They show an increasing passage energy barrier for increasing isoelectric surface overlap of molecule and pore in the transition state, elucidating that the electron density distributions of pore and molecule are rooted in the repulsion. Extending similar analysis to noble gases such as Ne, He, and Ar, Blankenburg *et al.* reported that noble gases follow a pathway of a minimum potential energy valley, attributed to attractive electrostatic interaction caused by the large polarizability of the noble gases.[12] $NH_3$ can also permeate following the minimum potential pathway due to its capability of hydrogen-bond formation with the hydrogen-terminated graphene pore edge. Also, the membrane can deform during the passage of gases due to their strong interaction, which lowers the energy barrier effectively compared with rigid pores. These findings support the fact that not only size comparison but also the various physical and chemical interactions between the graphene pore and the passing molecules can participate in the cross-graphene-pore gas transport mechanism. The pore deformation phenomenon has been subsequently investigated in more detail by Hauser and Schwerdtfeger for gases crucial in natural gas processing.[13] With a graphene pore system similar to Jiang and colleagues' pores, they observed that the pores adapt their size after removal of the benzene rings and they also monitored strong pore deformation during the passage of various gas species. For the nitrogen-terminated pore, they also observed a slight bending of the $CO_2$ molecule during the passage, explainable by a Lewis-acid–base mechanism of the charge distribution of bent $CO_2$ that shows a propensity for the Lewis-base nitrogen. The non-negligible interaction between transporting molecule and pore edge can cause molecular deformation during gas permeation. Thus, a simple comparison between molecular and pore sizes loses its significance beyond a first approximation of permeation/separation.

The first molecular dynamics (MD) simulation of gas transport ($H_2$ and $N_2$) across the graphene pore was carried out by Du *et al.*, scanning the pore sizes from 10 C equivalence to 32.[14] For the smallest pores, the pore size is smaller than the kinetic diameter of $N_2$, and so they observed no $N_2$ passage. Unexpectedly though, as pores opened up large enough to pass $N_2$, the calculated $N_2$ flow rate exhibited a superlinear proportionality with the open pore area, whereas $H_2$ followed the pore area scaling quite linearly. From the MD simulation, they found that a layer of $N_2$ molecules can absorb onto the graphene surface *via* van-der-Waals interactions, resulting in a surface

diffusion of the molecules that outpaces the ballistic diffusion. The unveiled surface adsorption and diffusion of gas molecules at pore dimensions slightly larger than the molecular sieving regime are of significant practical importance; for example, the surface diffusion mechanism could deteriorate an otherwise molecular-sieving-level separation factor or could enhance the selectivity toward strongly adsorbing species. Preferential adsorption onto the graphene surface has also been confirmed. According to an investigation of adsorption of $H_2$, $CO_2$, $CH_4$, and $N_2$, charge variation of the membrane surface has an influence on the physisorption of the gases.[15] A subsequent DFT calculation for hydrogenated pores with the size of two benzene rings added that the large quadrupole moment of $CO_2$ can be related to stronger adsorption to the graphene surface compared to $CH_4$, $N_2$, and $O_2$.[16] Further analyses by MD simulations found that linear molecules can absorb flat onto the surface and that $CO_2$ requires several events for the complete passage of the pore; for the passage, the adsorbate should be oriented properly to overcome the barrier, an event unlikely to happen to molecules approaching from the gas phase to the pore directly. These findings were simplified to a Langmuir adsorption model, leading to an argument that the surface-diffusion-related pore passage is the single, rate-limiting step. Competitive adsorption had a negligible impact on the selectivity because the gas adsorption did not fully saturate the membrane surface in the temperature and pressure ranges scanned in this investigation.

On the other hand, Drahushuk *et al.*[17] proposed a five-step analytical model by making an analogy of the surface-diffusion-incorporated transport to a surface-site-mediated catalytic reaction. The five identified steps are surface adsorption (on the feed side), pore association, pore passage (engagement), surface diffusion (on the permeate side), and surface desorption (detachment). Steady-state solutions of the differential equations of the analytical model for a range of graphene pore sizes from the 2-benzene-ring equivalent to the 32-carbon-atom equivalent suggested that ''pore passage'' is the rate-limiting step when the pore size is close to that of molecular sieves whereas ''surface diffusion'' can become the rate-limiting step for larger pores. They further predicted the importance of pressure-dependent permeance and the influence of feed composition due to competitive adsorption, in contrast to direct gas-phase passage. Sun *et al.* further compared the relative contributions of direct and surface diffusions for He, $H_2$, $N_2$, and $CH_4$ by MD simulation as a function of pore size.[18] The surface diffusion mechanism may contribute significantly to the entire permeation, such that its contribution could add up to being 16 times higher than the direct transmission part for transport of such a strongly absorbing species as $CH_4$ across a 12-C-removal equivalent pore. Surface diffusion may still take part in the *trans*-graphene transport, by at least an equal amount of contribution, for weakly interacting gases like He and $H_2$.

The effect of pore functional groups on permeation, a topic addressed briefly early on in the field, has been given renewed attention. Shan *et al.* looked into $CO_2/N_2$ separation across pores of 10–19 C atom equivalence by

MD simulations.[19] Pore functionalization with nitrogen could render the $CO_2/N_2$ selectivity as high as 11 for the otherwise unselective pores, attributable to a higher electrostatic interaction between the nitrogen edge and $CO_2$ rather than with $N_2$,, since $CO_2$ has a higher quadrupole moment. They also showed that functionalization of the membrane surface with hydroxyl groups could lead to preferential adsorption of $CO_2$ over $N_2$ by about seven times. These two findings agree with the previous observation that the selectivity toward $CO_2$ relies on the feed partial pressure of $CO_2$. Strong interaction among $CO_2$ molecules that can help to overcome the passage barrier turns vigorous with increased partial pressures.

The significance of the preferential molecular orientation in the *trans*-graphene passage noted earlier was confirmed by MD simulations. Solvik *et al.* examined the separation of various olefins and paraffins using all-hydrogenated pores of two-hexagon equivalence.[10,12,16,20] They considered in their simulation the free deformation of the membrane and its pores that had been recognized as crucial in the analysis yet often neglected. The simulation showed surface adsorption limited transport with preferential permeation, or separation, of ethene over ethane. Interestingly, the ethane, the molecule that adsorbs more, is permeating less compared to the less adsorbing molecule ethene. They explain their results by an unfavourable entropic energy barrier for ethane during passage. During the *trans*-graphene passage, molecules fall into a potential well, though ethane does not reside well inside the pore compared with ethene. The researchers decomposed the total barrier of the permeation rate model into activation enthalpy, surface adsorption, and entropic terms and observed that the activation enthalpy is similar, so that surface adsorption would in fact favour passage of ethane. However, the entropic barrier causes the ethene transport prevalence across the membrane. This finding is rationalized by the small size of the ethane molecule such that more configurations within the pore are possible during passage. Hence, it's entropic penalty is lower. Another MD simulation looking into the molecular orientation during the passage of $CO_2$ and $H_2S$ across 2–3-benzene-ring-equivalent, H- or N-functionalized pores found that the linear $CO_2$ molecule follows a narrow range of orientation during passage.[21] The radial density distribution extending out of the pore exhibits an accumulation zone within the pores, surrounded by an ~0.5-nm-wide depletion zone, which eventually transitions into a peripheral zone of constant adsorption density. Starting from the adsorption zone, the molecules feel no concentration gradient and thus accumulate homogeneously. Near the pore, on the other hand, a concentration or density gradient develops in the pore, along which molecules diffuse.

Recently, another aspect of permeation across subnanometre openings has been predicted by combined DFT and MD simulations of $CH_4$, $CO_2$, and $N_2$ separation.[22] The barrier against the molecular passage consists of a combination of pore entry and exit barriers and varies depending on the pore, functionalization, and the passing molecule. For example, $CO_2$ usually occupies a potential well within the pore. To leave the pore, the molecule

must escape the potential energy barrier. Once charge is imposed at the pore edge, its strong interaction with the $CO_2$ quadrupole can adjust the transport energy barrier against $CO_2$. This mechanism provides an additional means of separation other than size exclusion or hindered diffusion and may be particularly relevant for similarly sized molecules.

It is interesting to consider the effect of a non-permeating species in a gas mixture on the permeance of a permeating mixture. Wen *et al.*'s MD simulation delved into this question using $CH_4$ as a non-permeating species and $H_2$ and $N_2$ as permeating species through a 13-C-atom-missing pore.[23] The presence of $CH_4$ can decrease both permeances of $H_2$ and $N_2$, and this effect can be more severe for $N_2$. They attribute this to two contributions: competitive adsorption and pore blocking. Competitive adsorption is more severe for $N_2$ as $H_2$ barely adsorbs to the surface. $N_2$, on the other hand, tends to adsorb significantly and puts itself into competition with $CH_4$, resulting in less surface occupancy than in the absence of $CH_4$. Besides, the number densities of both $H_2$ and $N_2$ can increase near the pore, though the permeation is curbed by the presence of $CH_4$. According to their explanation, $CH_4$ may partly occupy the subnanometre pores and slow down the transport of $H_2$ and $N_2$ effectively. The combined effect of the competitive adsorption and the pore blocking can result in decreased permeance in the presence of a non-permeating species, implying practical importance in gas separations in which more than two species are often present.

Overall, the available literature revealed various facets of the permeation mechanism of gaseous molecules across porous graphene membranes. Besides an energy barrier resulting from an interaction between a subnanometric pore and transporting molecules, in association with electron cloud overlapping, adsorption of the molecules to the graphene surface and subsequent surface diffusion have a significant influence on the permeation and selectivity of the graphene membranes with subnanometric pores. Furthermore, the effects of the pore and surface functionalization, an entropic barrier based on orientation restriction, as well as the mixture effects such as competitive adsorption and steric hindrance (*i.e.*, pore blocking) can altogether play a non-negligible role in *trans*-graphene membrane transport. It is noteworthy that various simulations predict a wide range of permeance and selectivity values, calling for verification to clarify the deterministic transport mechanisms and to ultimately quantify membrane performance for gas separation.

In this light, the experimental understanding of the mass transport across porous graphene membranes can fall into two categories. The first category comprises publications based on mechanically exfoliated graphene flakes that are high in quality but only as wide as tens of micrometres. With these systems, it was possible to study impermeability of and transport across subnanometric pores on graphene in the molecular sieving regime. The second category covers publications based on the graphene grown by chemical vapour deposition (CVD) and incorporating intrinsic or artificial

pore formation. CVD can synthesize potentially large-scale membranes and is considered the most promising manufacturing method for real graphene membrane applications. The large area allows for various manufacturing options for the graphene perforation and the membrane formation. Intrinsic defects and ruptures of the synthesized graphene could be a drawback of this approach during membrane manufacturing, but they can provide a molecular transport pathway per se.

The prerequisite for studying the transport across porous graphene is the impermeability of the pristine graphene demonstrated by Bunch and colleagues.[5] Employing the same method, Koenig *et al.* pressurized mostly bilayer graphene blisters by applying UV-oxidation etching.[24] If well controlled, this treatment may enable the formation of pores in the subnanometre dimension, a characteristic size regime useful for molecular sieving of various gases. The transport rates were either measured by AFM tracking of the membrane deflection over time or by a temporal change in resonance frequency of the membrane while transporting gases. They reported giant selectivity between $10^3$ (for $H_2$/Ar) and $10^4$ (for $H_2/N_2$) of the UV-oxidated bilayer graphene membrane as well as size exclusion of $SF_6$ having a kinetic diameter of 4.9 Å. The measured permeance matches the prediction of Blankenburg *et al.* of a H-passivated, 6-C-atom-equivalent pore, but interestingly, their selectivity of 2 for $H_2/CO_2$ differs significantly from the theoretical prediction ($10^{17}$).

Further work of the same group with a monolayer graphene blister having subnanometric pores has revealed that He permeance can vary by a factor of ~5, if the membrane surface is irradiated with a laser of 2–2.3 eV photon energy.[25] Additional laser shining could return the permeance to its initial value. They attributed this switchable permeance to the presence of gold nanoparticles that had been evaporated onto the surface. According to their speculation, energy input such as photon irradiation could induce surface migration of Au NPs to block the subnanometric pores. However, what remains to be clarified is a negative control of this permeance switching phenomenon for a graphene membrane without the nanoparticles on it.

Actually, this paper reported stochastic Ne permeance switching of monolayer graphene in the absence of the surface nanoparticles. Their subsequent work provides the Hidden-Markov-model-based analysis of this stochastic permeance switching of three monolayer graphene pores that can switch their individual permeance values between ''high'' and ''low'' states.[26] For gas species having kinetic diameters larger than that of He, the permeance shows various discrete levels that can be mathematically modelled by this binary state system of the three pores. From the switching frequency, the authors could estimate the activation energy value of 1 eV required to switch the permeance state, consistent with the energy barrier of *cis–trans* isomerization rearrangements. Interestingly, this energy is less than the laser photon energy previously reported to switch a molecular valve from ''high'' to ''low''.[25]

Due to the size limitations of graphene flakes, mechanical exfoliation has not been considered realistic for membrane applications outside a laboratory. Instead, CVD-grown graphene can potentially take as large a dimension as a few metres such that its use as a large-scale gas separation membrane is feasible. Boutilier *et al.* investigated the feasibility of achieving gas selective graphene membranes despite the presence of non-selective defects, ruptures, and incomplete graphene coverage of the support structure.[27] They could show an exponential decrease of leakage pathways across CVD-grown graphene as well as increased gas permselectivity for multiple layers of graphene, confirming that both the total amount of leakage as well as the average size of the leakage path can diminish if multiple layers of imperfect CVD-grown graphene are stacked atop one another. In order to predict the selectivity of graphene, a model was proposed considering a membrane that possesses hypothetical, highly selective subnanometric pores and lies on a porous support, a membrane architecture so-called a thin-film composite. This model illustrates that, despite the presence of unselective defects in the graphene, it is possible to obtain a highly selective membrane as long as the contribution of the unwanted defects is negligibly small. The authors argue that the support should slow down the non-selective transport through ruptures and only slightly reduce overall selectivity.

Later, they used the comparable transport impedances of graphene and the support layer to show enhanced Knudsen diffusion permselectivity of an ion bombarded and subsequently PDMS spin-coated PDMS/graphene/PCTE composite.[28] A further study used trilayer graphene on 20-nm-pored anodic aluminium oxide (AAO) that was etched in $O_2$ plasma for various durations. Single-gas permeance measurements revealed a permselectivity above Knudsen, indicative of molecular sieving.[29] However, the contribution of unselective broken graphene with potentially highly selective subnanometric pores in graphene hampers the unambiguous characterization of the graphene pores. Therefore, a model was utilized to estimate the selectivity of graphene pores in the subnanometric regime, when accounting for effects of ruptures and imperfect coverage of the graphene layer. The model predicts $He/SF_6$ selectivity ranging from 10 to 400 depending on the fabrication conditions. The permeance of their measured composite membranes is quite small due to the small pores of the support membrane such that it is comparable to permeances of $<$100-nm-thick polymeric membranes. Consequently, these composite structures cannot meet the promise of ultimate permeation of atomically thin membranes. These studies highlight the significant challenges of gas separation using porous graphene on macroscopic areas and suggest strategies to overcome these difficulties.

As the thickness of a pore approaches zero, transport physics will drop out the channel-length dependency along with one pore-width dimension, thus avoiding the singularity – an infinite mass flux – of the Fickian dynamics. The transport dynamics enters into non-Fickian physics. In a continuum mechanics regime, where this zero-thickness pore measures an opening size far in excess of the molecular interaction length scales, a Stokes flow model

can provide analytical solutions. For a pressurized fluid flow across an opening through a 2D disc, for instance, the linear relation between the flux and the pressure forcing has been analytically obtained in the form of Sampson's formula.[30,31] In the Sampsonian dynamics, the mass flux of a fluid is linearly proportional to the pore opening size (diameter) and the pressure force, inversely proportional to the fluid viscosity, and invariant to the pore length (or depth). On the other hand, in a molecular flow regime, where pore size is comparable to or far smaller than the molecular interaction length scales, a ballistic transport model such as effusion or the dusty gas model can describe the transport dynamics. Effusion can occur for a gas species when both the pore size and the depth are much smaller than the mean free path of the species. The simplest description of effusion is related to the Boltzmann gas dynamics; the mass flux across an aperture on a thin wall is proportional to the disparity in the product of gas density and thermal velocity. As a result, the effusive transport flux from one side to the other depends linearly on the pressure and is inversely proportional to the square roots of molar mass and temperature. Inherent to the nature of the free molecular transport, the flux from one side to the other is independent of the counter flux, and thus the net flux is determined by the difference in both types of flux.

It has been difficult to verify these flow theories and characterize them experimentally because of the deficiency of a method for manufacturing a nearly zero-thick pore. Characterization of the ballistic effusion could have been made in the high vacuum setup, yet this capability is still bounded to the Knudsen diffusion limit if pore depth cannot be made ultrathin. One fundamental limit of the material thickness is an atom, and it is graphene, one of the ideal 2D materials, that has the mechanical, physical and chemical potential to demonstrate zero-thickness pores. Still, the primary difficulty in the verification of the aforementioned flow theories and the characterization of the nature of the length-invariant transport physics lies in the method of perforating the variously sized pores accurately on the graphene in its unsupported, self-sustaining configuration.

Researchers have recently developed a physical perforation method for freestanding graphene to investigate this length-invariant mass transport across graphene pores in a wide range of transport regimes from free molecular to continuum. Celebi, Buchheim *et al.* applied the focussed ion beam (FIB) technique to drill well-defined pores with diameters ranging from sub-10 nm to 1000 nm on freestanding double-layer graphene (as thick as approximately two C atoms).[7] Preparation of a myriad of similarly sized pores can facilitate the direct atmospheric characterization of the gas transport rate across, for example, pores smaller than the gas mean free paths. With this technical breakthrough, they verified that the effusion mechanism dominates transport in the free molecular regime, whereas in the continuum flow regime of larger pores, a modified Sampson's formula describes the non-Fickian dynamics. Furthermore, a transport minimum at a Knudsen number around unity, often observed for finitely thick channels and

ascribable to gas-and-pore-wall friction, was unobserved for the graphene pore, confirming the unique transport mechanism across the 2D pore. Gas permselectivity is scaled to the inverse square root of molar mass just as predicted by Graham's law of effusion.

Despite the theoretical and experimental investigations that have revealed many findings on the gas separation behaviour and the transport mechanism across porous graphene membranes of various pore sizes, important questions still remain unanswered. Particularly for graphene membranes with few-nm to sub-nm pores, a unified picture of selectivity and permeance remains to be established considering the interplay of molecular-level interactions among the membrane, permeating gas, and other gas species. The effect of surface diffusion may cause a deviation from ever larger selectivity for ever smaller pores, as predicted for $H_2$–$N_2$ separation for sub-nanometric pores. Figure 3.1 shows a comparative analysis of the $H_2$–$N_2$ separation factor for pores of various sizes and sources. The separation

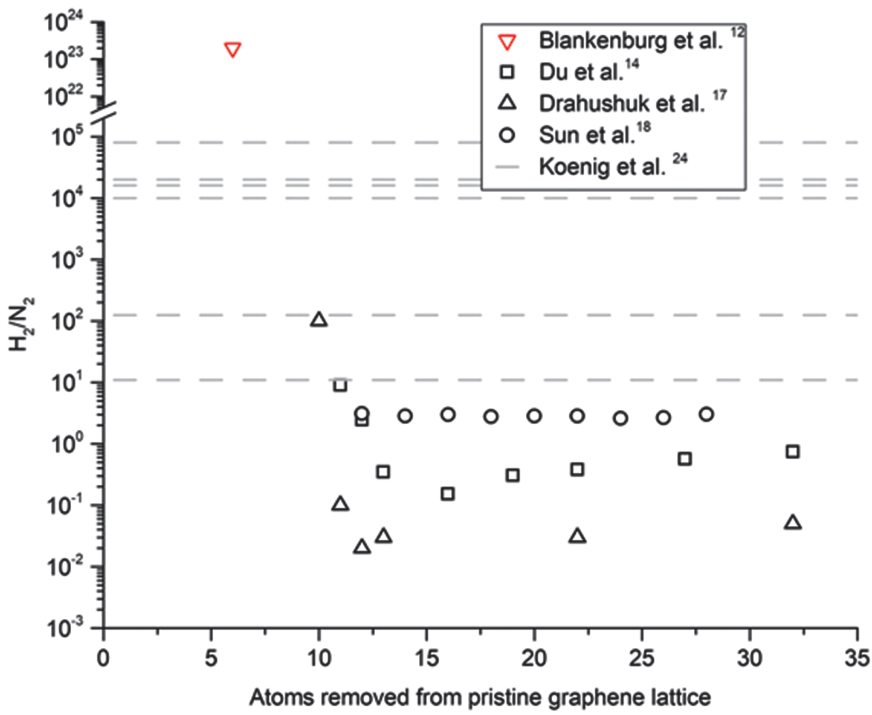


**Figure 3.1** $H_2$–$N_2$ selectivity values from various simulations and experiment, with respect to graphene pore size (number of C atoms removed from a graphene crystal). A strong disagreement exists among simulations for pores with size equivalence of more than ten C atoms. Symbols represent the corresponding study; colours represent chemical group at the pore edge. Black and red represent no and hydrogen functionalization, respectively. Grey represents unknown functionalization.

factor predictions vary rather largely by up to two orders of magnitude and also conflict with one another with respect to the transport favouring species: *i.e.*, hydrogen-selective or nitrogen-selective. This uncertainty needs clarification about the true separation factor of pores near 1 nanometre in size. Furthermore, the membrane-based gas separation application demands the actual molecular sieving selectivity of CVD-grown defective graphene in the practical mixture separation process. Following this reasoning, the challenge of scaling up the membrane area needs to be taken up, as practical membranes will require membrane areas ranging from metres to even thousands of metres, although this argument remains to be further discussed in the community. For subnanometric pores, the self-healing phenomenon can pose a great challenge to the membrane lifetime.[32] Here, effective approaches for pore edge stabilization by functionalization or other means need to be established.[33,34] Eventually, porous graphene membranes need to compete with other types of gas separation membranes such as zeolites, carbon molecular sieves, carbon nanotube membranes, graphene oxide, metal organic frameworks, and others.[1] Chemical stability, mechanical strength, temperature and pressure requirements, as well as an appropriate support material, need to be investigated to find the best suited material for a targeted gas separation application.

## 3.3 Liquid Transport Across Porous Graphene Membranes

Liquid transport across porous graphene membranes is of interest not only for the fundamental understanding of transport phenomena but also for various applications potentially encompassing from filtration and desalination to biomedical engineering processes such as dialysis and DNA sequencing.

### 3.3.1 Water Transport Across Porous Graphene Membranes

The transport of water across graphene membranes was investigated in Suk and Aluru's MD simulation that considered 0.75-nm-wide and 2.75-nm-wide pores on graphene, and the results were compared to the state-of-the-art fast water transport through carbon nanotubes (CNT).[36,37] A very small (~0.8 nm) pore of graphene can transport water at a slightly slower rate than that of a similarly wide CNT conduit, which is related to the frequency of water dipole rearrangement during the passage. For both graphene- and CNT pores, water molecules take a single-file configuration in transporting in these tiny pores. However, water molecules in the 0.8-nm-wide CNT keep a single dipole orientation most of the time during the passage, while water dipoles in the graphene pore can frequently alternate in a rather random orientation. This fluctuation in the dipole orientation requires energy, and thus transport in the subnanometric graphene pores can occur at a slower rate than the water

conduction across a CNT with a similar diameter. Across 2.75-nm-wide pores, on the contrary, the simulation resulted in water transport rates faster for graphene pores than CNTs. Unlike a pluglike profile in the CNT, the velocity profile of the water flow demonstrates a reportedly[37] parabolic profile in the graphene pores. A follow-up simulation investigated water transport across graphene pores with various diameters from subnanometre to ~4 nm diameter and tried to see if it can be modelled with a continuum dynamics theory: an adjusted Hagen–Poiseuille (HP) equation.[35] Instead of the membrane length (0.54 nm), a pore-diameter-dependent hydrodynamic membrane length was utilized with accounting for entry and exit pressure losses, which occur before and after the pore. Regarding the total flow enhancement, the authors observed an increase in slip length that is in competition with an increase in water viscosity for nanometric pores. According to the authors' claim, it is a layered configuration of a water H-bond network in front of and behind the graphene nanopore that can lead to a decrease in the cross-pore water diffusion coefficient, ultimately increasing the water viscosity during the passage. The layering may thus reduce the probability of a water molecule to transmit from one water layer into another, thus resulting in an increased water viscosity.

Another study focussed on water transport across graphyne, a related structure to porous graphene, found an even stronger increase in the water viscosity that is inversely proportional to the sixth power of the graphyne pore characteristic length and attributed to attractive forces stemming from the Lennard-Jones potential that induces stronger H-bond orientation within the first few water layers directly over the membrane surface.[38] Even though the earlier report by Suk and Aluru[35] showed qualitative results of water viscosity in nanoconfining graphene pores as well, quantitative scaling differs between these two studies, which demands further investigation for the exact scaling and mechanism and also for the validity of the water viscosity alteration hypothesis itself.

The effect of pore functional group, which had been excluded in the previous study, was taken into account by Cohen-Tanugi and Grossman for pore sizes in the subnanometric regime possibly suited for desalination.[39,40] Hydrogenated and hydroxylated pores were compared. It was found that hydrogenated pores transport water significantly less than the hydroxylated pores for a comparable open pore area. They attributed this finding to a smaller chance of H-bonding between transporting water molecules and the hydrogenated pore edge such that the water molecules transfer across the pore in a more ordered manner. This picture can be interpreted as an entropic barrier imposing an (activation) energy penalty for the water passage across the subnanometric pores of graphene.

Water transport across graphene pores in the continuum pore-size regime was probed experimentally by Celebi, Buchheim *et al.* who prepared precise pore sizes from 50 nm to 1000 nm *via* FIB drilling on freestanding graphene.[7] They demonstrated that the unique transport properties of a double-layer CVD graphene membrane cannot be described accurately by

the HP formalism, but instead, the transport physics follows the model proposed by Sampson. They were able to demonstrate that resistance to water permeation across the pore is accurately described by considering the entrance resistance alone, while pore passage resistance is negligible, a conclusion in agreement with the Sampson's formula. Mathematically, the pore-size scaling of the cross-2D-opening transport follows the third power of the pore diameter instead of the fourth power that the HP formalism demands.

Figure 3.2 shows measured, simulated, and analytical predictions of the per-pore-permeance of water across nanopores in porous 2D barriers. Sampson's theory can be seen to describe transport accurately for all pore sizes, while the H–P equation significantly deviates from experimental values for any pore larger than a few nanometres.

### 3.3.2 Ion Transport Across Nanoporous Graphene

The study of the transport of an ionic solute across nanoporous graphene membranes is relevant in various technologies such as desalination, biomedical applications, batteries, and fuel cells. Therefore, significant efforts have been made to understand and control ionic solute passage or rejection with nanoporous graphene membranes.

The first computational study in 2008 considered the transport of an ion solute across two distinct subnanometric graphene pores, one with a hydrogen-terminated edge and the other having an edge terminated with fluorine (F) and nitrogen (N).[41] Based on an electronegativity argument, the hydrogenated pore is expected to be slightly positively charged, while the F–N functionalization would cause negative charges to face the pore centre. Under an external electric field, the F–N functionalized pores show cation selective transport, and the hydrogenated pores are anion selective. Transport of various ions shows transmission rates consistent with the hydration radii of the ions considered ($Li^+$, $Na^+$, $K^+$, $F^-$, $Cl^-$, $Br^-$), indicating possible size selectivity. Electrostatic attraction determines whether the respective ion–pore combination enables entry and passage through a given pore, while the transport efficiency (or rate) depends on the size and the energy penalty associated with the hydration shell of each ion. Consequently, this study revealed the potential of a subnanometric graphene pore to act as an ion gate. A later study extended the analysis to larger pores up to 2 nm in diameter and thus simplified it by ruling out the size selectivity.[42] Still, the authors observed ion selective transport in these sub-2-nm pores if the pore edge is charged properly. Negative charges will facilitate cations while impeding the passage of anions, in agreement with the previous study. This behaviour is reminiscent of the Donnan exclusion theory in which counterions have a higher concentration within the membrane than in solution due to electrostatic interaction between the ion and pore charges. Interestingly, the ion selectivity trend is still maintained even though the Debye

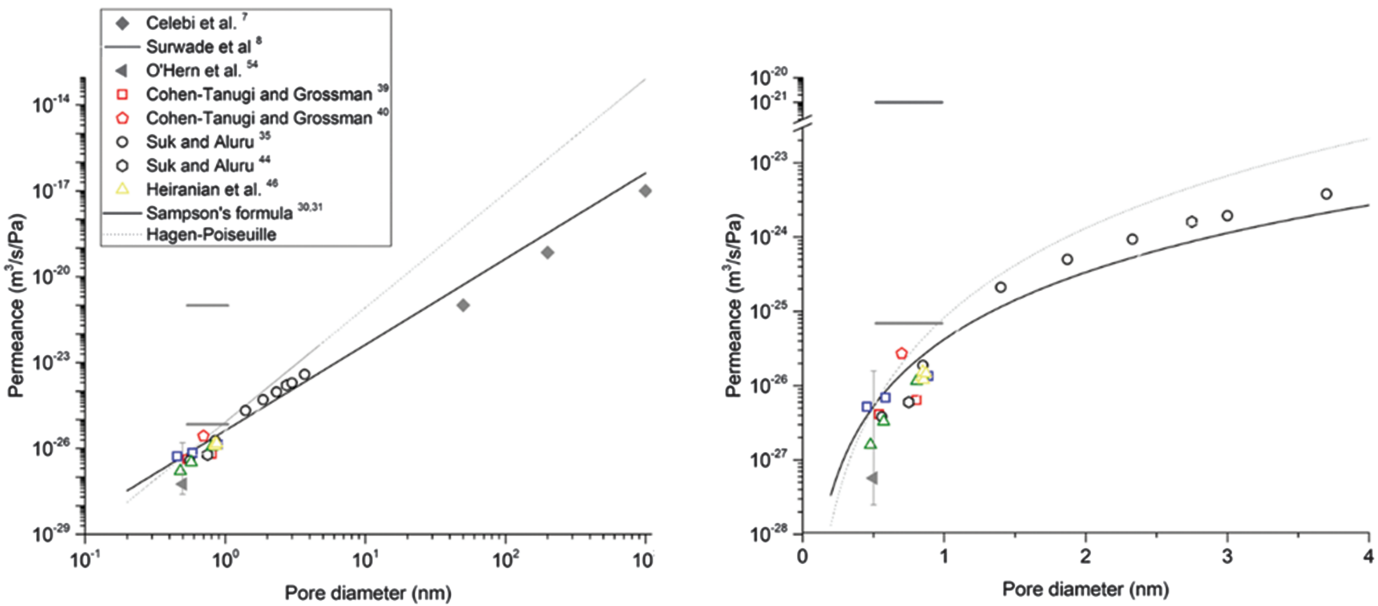


**Figure 3.2** Per-pore-permeance as a function of pore diameter of various simulation and experimental data. Sampson's formula is accurate for all pore diameters, contrary to the Hagen–Poiseuille formalism. Symbols represent the corresponding study; colours represent chemical group at the pore edge. Black and red represent no and hydrogen functionalization, respectively. Grey represents unknown functionalization. Dark red represents molybdenum edge atoms and green represents mixtures of molybdenum or sulphur atoms. Green and dark yellow represent Mo only and Mo–S-mixed pore edge atoms in $MoS_2$. A water density of 1 g cm$^{-3}$ is assumed unless the respective study provides more information.

screening length is much smaller than the pore diameter (~0.3 nm), raising a question that calls for additional investigations.

Analysing the ion transport across non-functionalized, uncharged pores with sub-5-nm diameters, Suk and Aluru looked into ion conductance and mobility through MD simulation.[43] They reported physical chemical aspects of aqueous ion solutions within these pores. In detail, they found that the number of water molecules within the first hydration shell of $K^+$ and $Cl^-$ ions remains constant for pore sizes up to 1 nm. Smaller pores show a reduced coordination number that is attributed to steric exclusion and dehydration effects, however the coordination number reduces only slightly, indicating that a passing ion can compose its hydration shell from water molecules from both sides of the atomically thin graphene membrane. Simultaneously, the pore conductance decreases due to both causes: a lowered concentration of ions within the pore and a reduced ion mobility near the pore. The lowered concentration originates from a combination of steric hindrance and hydration energy penalty, while the ion mobility is reduced for ever smaller pores due to impeded ion diffusion. The impeded ion diffusion is attributed to the water layering configuration on both sides of the pore, as reported in a previous simulation.[44] These diameter-dependent concentration and mobility factors collaborate to change the nanopore's ion conductance from the value predicted on the basis of the bulk properties, if the pore diameter approaches a subnanometric dimension. For pores smaller than 9 nm in diameter, the continuum model description becomes erroneous such that their empirically derived diameter-dependent properties should be applied for an accurate description of graphene pore conductance.

Insight into selective ion passage across subnanometric graphene pores can also help to understand biological ion channels, as shown by He *et al.*'s MD simulation.[45] By mimicking biological ion channels by way of attaching carbonyl or carboxylate groups to the pore edge, it is possible to achieve preferential $K^+$ transport over $Na^+$ as is seen in biological ion channels under applied bias. Under applied voltage bias, $K^+$ is coordinated by one carbonyl group more than $Na^+$ and thus it is selectively transported, as the experienced passage barrier of $K^+$ is smaller than that of $Na^+$. Furthermore, $Na^+$ is observed to bind more strongly to carboxyl groups than $K^+$, leading to preferential $Na^+$ passage over $K^+$ in the smallest pore at low voltage, since the bound $Na^+$ blocks $K^+$. $Na^+$ is transported by a knock-on mechanism and due to the stronger $Na^+$ interaction with the pore-edge functional groups, it is more likely to be replaced by a new $Na^+$ rather than a $K^+$. Therefore, $Na^+$ selectivity can result. At high voltage, however, $Na^+$ cannot block the pore anymore, since the carboxyl group reacts to the larger electric field by swinging out of the graphene plane. Then, $K^+$ ions are not blocked from passage anymore, and since $Na^+$ is attracted strongly to the pore edge, its permeation rate decreases.

Graphene's potential to selectively transport ions also raises the question about complete ion rejection that would imply a membrane feasible for

desalination applications. Cohen-Tanugi and Grossman delved into this question by means of MD simulation for various subnanometric pores functionalized with $OH^-$ or $H^+$.[39,40] For effective pore diameters above 0.55 nm, the pores lose their rejection capability, but below that threshold, selectivity up to 100% can be achieved. At a given pore size, hydroxylated pores show lower rejection of salt ions, possibly attributable to the H-bond between hydroxyl groups and hydration-shell water; the free energy barrier could be lowered if water molecules from an ion hydration shell could be replaced by a hydroxyl functional group at the pore edge during the passage, a mechanism the hydrogenated pore is missing. Interestingly, the subnanometric graphene pores lose the ion rejection capability as pressure increases. The authors hypothesized that the larger the effective volume of an ion hydration shell, the more sensitive the graphene pore becomes to a pressure increase, however, facilitated dehydration of salt ions during passage at higher pressures may also explain this observation. Furthermore, the simulation conditions render water in the compressible regime, which may have an effect on the salt hydration layer. Still, linear extrapolation of salt rejection of a 0.8-nm-wide pore to practical pressures (*e.g.*, 5 MPa) results in nearly 100% salt rejection, which raises the question of how salt rejection and pore size are related at lower pressures and the possibility of desalination with pores larger than that stated in this study.

Apart from graphene, other 2D materials show similar promise for high permeation due to their thinness. An MD study of water desalination across nanopores in monolayer molybdenum disulphide ($MoS_2$) in fact revealed 70% higher permeance than that across graphene pores.[46] The unique structure of $MoS_2$ allowed for comparison of three different pores with Mo-only, S-only, or a mixture of those atoms to be located at the pore interior. A pore with Mo edge atoms shows the fastest transport, while pure S atoms are the slowest transporters of water. A difference between these pores is that Mo pores have an hour-glass cross section due to the atomic structure, while S pores do not have this geometry. The authors attribute the fast flow to this hour-glass geometry and furthermore to hydrophilicity of the Mo sites. However, the application of the concept of hydrophilicity and hydrophobicity at the atomic level is questionable, as the hydrophilicity of materials at the macroscale can change significantly under nanoconfinement or structuring. Although the authors agree with Cohen-Tanugi and Grossman in that faster permeating pores reject less ions, their simulation shows around 95% rejection for both $MoS_2$ and non-functionalized graphene, while Cohen-Tanugi reported merely ~40% rejection for similar pore sizes and pressures.[39,40] Such a remarkable difference demands further investigation of the true rejection capability of atomically thin membranes for a given pore size, pressure, and chemical functionalization. The authors further extended the analysis to other transition metal dichalcogenides to observe that mainly the metal component dominates the permeation and salt rejection capabilities.

The first experimental characterization of ionic transport across nanoporous graphene was published in 2010 by Garaj *et al.*[47] They showed the nanopore conductance of CVD graphene to be almost linearly increasing with diameter. From their conductance measurements with various pore diameters, it was possible to extract the effective insulating membrane thickness to be 0.6 nm, a value that was confirmed by DNA translocation measurements with a ~5-nm-wide pore and matches well with the theoretical work of Suk and Aluru.[43] Using the DNA translocation experiments, they could show subnanometre resolution of graphene for DNA discrimination, rendering atomically thin porous graphene a promising candidate for DNA sequencing applications.

Extending the analysis of the ion conductance to pores up to 2 nm, Jain *et al.* characterized a current-voltage behaviour across intrinsic defects of CVD graphene, in resemblance to biological ion channels.[48] A Nernst–Planck model incorporating electrostatic and steric interactions of a graphene pore of variable diameter and charge with a single ion could allow the transport properties of the pores to be extracted. Linearity between current and voltage is attributed to uncharged pores with diameters above the hydrated diameters for the ions such that a charge-neutral pore with pore size larger than the ion hydrated radius cannot impose steric hindrance on the passing ion. Voltage-activated behaviour could be attributed to uncharged nanopores that sterically hinder the passage of the hydrated ion. The nonlinear current increase above a certain threshold voltage may originate from increased ion dehydration due to the higher electric-field driving force. At small electric fields, the dehydration barrier strongly impedes ion passage leading to small currents. The presence of charge at the pore mouth may alter the transport in two possible ways: a charge that is positioned symmetrically could result in the current-saturation behaviour by imposing electrostatic repulsion on passing ions, while an asymmetric placement of the charge at the pore mouth yet out of the pore plane could produce a rectified current–voltage characteristic. Here, the asymmetric placement may couple the perceived near-pore electric potential toward the direction in which an ion permeates, causing an asymmetric current–voltage behaviour. In some cases, rapid current fluctuations are observed for samples that otherwise show the voltage-activated behaviour. This current fluctuation is attributed to a protonation–deprotonation transition because of time-scale similarity and power spectra analogous to those obtained for the protonation–deprotonation transition. What is not clear, though, is the otherwise voltage-activated behaviour for these devices that was previously attributed to steric hindrance in the absence of charge, while protonation induces pore charge alteration. This seemingly conflicting behaviour calls for further examination. Still, the remarkable similarity to transport in biological channels lends graphene nanopores eligibility as a model platform to mimic biological ion channels.

The smallest nanopore thus far probed for ionic transport is ~0.3 nm in diameter perforated into single layer $MoS_2$ membranes.[49] Opening pores in

$MoS_2$ by electrochemical means allowed for controlled fabrication of single pores in suspended $MoS_2$. For a 0.6-nm-wide nanopore, current–voltage characteristics show negligible current below a certain threshold voltage upon which the current non-linearly increases. The voltage range in which current is suppressed depends on the pore size and the cation valence that passes through the pore. The nanoelectronics concept of a Coulomb blockade is applied to ionic transport to explain the observed phenomena. This model dictates that an individual ion can block a nanopore, stopping other ions from passing through it, yielding negligible current at a small bias. Increased voltage bias can release this blockade through a mechanism whereby augmented electrostatic interaction between cations in the vicinity of the nanopore eventually removes the cation from the pore. Negative charges at a nanopore could cause cations to bind to it, resulting in current blockade. By changing the pore size, the authors argued that a dehydration energy penalty of ions dominates the current blockade for sub-0.6-nm-wide $MoS_2$ nanopores while justifying an ohmic current–voltage behaviour for super-1-nm-wide nanopores that are too large for a single ion to block them. Their observed current-voltage characteristics also resemble biological ion channels of dimensions similar to their nanopores.

These researchers furthermore employed concentration-gradient-driven selective ion diffusion across an individual nanopore on monolayer $MoS_2$ to demonstrate a power generator.[50] With pores ranging from 2 to 25 nm, selective ionic passage could be achieved, attributed to negative surface charge evidenced by conductance saturation at low concentration and increased conductance at higher pH. The surface charge is capable of screening anions due to the significant Debye length (~10 nm) resulting in a net positive current following the concentration gradient. The smaller the pore, the higher the ion selectivity of the nanopore, resulting in a larger voltage generated at the expense of smaller current. Similarly, the lower selectivity of a larger pore induces lower voltage yet at larger current, a trade-off that hints at an optimal nanopore size to maximize power generation. If a membrane bears nanopores with an average pore diameter of 10 nm at 30% areal porosity, it may potentially generate as great a power density as 1 $MW\,m^{-2}$ thanks to efficient transport across the atomically thin membrane. However, a sub-additive ion–current increase may be expected as well for 2D porous membranes, as has previously been observed for solid-state nanopores.[51]

While the role of surface charge on $MoS_2$ that screens ion passage is based on the Debye layer thickness, Rollings *et al.* probed selective ionic transport across graphene nanopores where the Debye layer is much smaller than the pore size.[52] For up to 50 nm-in-diameter pores, $K^+$-to-$Cl^-$ selectivity neared almost 100 and relies on the solution/electrolyte pH, suggesting a mechanism of protonation–deprotonation of chemical moieties at the pore edge. A pH scan revealed that the graphene nanopore edge is negatively charged at neutral conditions. However, since the Debye screening length (1 nm) is much smaller than the pore diameter and

charge screening alone from the pore edge cannot explain the observed selectivity, another mechanism for selectivity needs to be conceived. Ion selectivity of pores much larger than the Debye screening length is rationalized by the negative surface charge of graphene that can attract a mobile cloud of screening cations. These mobile cations can diffuse along the graphene surface and cross around a pore edge, causing net ionic current to be cationic. This hypothesis is supported by conductance measurements at pH 8 and 2 that show higher transmembrane ion conductance at pH 8, indicating that more cations screen the negative surface charge of graphene than in the pH 2 case. Numerical solutions of Poisson–Nernst–Planck (PNP) equations for a surface charge density of null and $-0.6\ \mathrm{C\,m^{-2}}$ confirm that results of the strong negative charge case agree with the measurements well. In comparison to Feng *et al.*, Rollings *et al.* reported that an approximately 10-fold higher surface charge may result in great selectivity even at a pore diameter of 50 nm.[50] The origin of the surface charge is not fully understood but may be related to their sample preparation method involving voltage pulsing, given that other researchers have reported much weaker selectivity at smaller pores.[9]

Complete ion rejection across subnanometric pores of monolayer graphene has been reported by Surwade *et al.*, implying the potential of graphene as a water desalination membrane.[8] Subnanometric pores could be created by $O_2$ plasma treatment, as evidenced by aberration-corrected scanning transmission electron microscopy. By contacting one side of the graphene membrane to deionized water at 40 °C, they measured extremely high mass flux across the $O_2$-plasma-treated graphene membrane, which is surprising and calls for further investigation of phase change under nanoconfinement. Subsequently, ionic current measurement of this membrane (0.5–1-s-long $O_2$ plasma treatment) obtained none to very low ion conductance, indicating ion rejection and the potential as an effective desalination membrane. Repeating the initial permeation experiments with an ionic solution shows much slower water permeation and almost complete ion rejection for $<1$ s plasma treatment time. Osmotic water flow experiments further revealed the semipermeable nature of the membranes and their desalination capabilities. The osmotically driven water transport rate occurs exclusively in the liquid phase and matches well with theoretical predictions.

Any real membrane for liquid-phase separation applications is likely to be grown by CVD and of macroscopic size. Membranes prepared in this way often accompany intrinsic defects such as pinholes from graphene growth or ruptures from membrane fabrication. As was similarly probed for gas transport, O'Hern *et al.* investigated transport across intrinsic defects of graphene over a macroscopic area of $O(10)$ mm.[27,53] They found an inhibited transport of TRMD (*ca.* 12 nm in size), while those of KCl, allura red, or TMAC were not significantly affected, when the permeance values were corrected for uncovered bare PCTE areas. This reveals the presence of intrinsic defects of 1–15 nm in size, as is confirmed by electron micrographs. Control over subnanometric pore sizes in a potentially scalable process was

achieved in a later work using first energetic ion bombardment of CVD graphene with subsequent wet chemical etching to grow defects into permeable pores.[9] For a certain etching time, it was possible to demonstrate enhanced KCl transport compared with allura red, supporting a size exclusion argument and indicating the generation of pores larger than KCl (0.7 nm) but smaller than allura red (1 nm).

Since macroscopically grown CVD graphene often contains both intrinsic defects and ruptures originating in membrane handling, a two-stage strategy can be applied to seal membrane defects.[54] In the first stage, atomic layer deposition (ALD) of *ca.* 3.5 m thick hafnia ($HfO_2$) was applied targeted to close defects below 15 nm in size, after which interfacial polymerization (IP) of nylon-(6,6) was utilized for sealing larger defects that originate from ruptured graphene on a 200-nm-pored PCTE support. Subsequent etching by potassium permanganate can create pores with an average value of 0.16 nm, as analysed by HRTEM, with a small fraction of pores larger than the water van der Waals diameter and rarely salt permeable pores (>0.7 nm). Osmotic pressure experiments show water transport close to theoretical prediction and of a similar order of magnitude as polymeric membranes typically applied in reverse osmosis. Solute rejection was studied with NaCl, $MgSO_4$, allura red, and dextran showing negative rejection of NaCl (0.7 nm), and rejection of 70% $MgSO_4$ (0.8 nm), 90% allura red (1 nm), and 83% dextran (3.7 nm). Negative NaCl rejection is equivalent to more NaCl transport through their graphene/PCTE composite in comparison to the bare composite, according to the used rejection definition. This observation along with the lower dextran rejection despite the larger size requires further study and might be related to the KCl permeability of nylon.[55] Further, the role of pores too small for IP sealing and too large for ALD sealing remains unclear.

To target applications properly, achievable salt rejection as a function of the pore diameter needs to be understood. Figure 3.3 shows various experimental and theoretical results for various nanopores. In general, pores below 0.5 nm are found to reject salts such as NaCl, however for pores slightly larger than this size, the rejection decreases but also becomes inconsistent within a pore size. While some research predicts over 98% rejection of *ca.* 0.85 nm pores, others simulate down to a mere 30% rejection at a given pore size. Differences in chemical functionalization of the pores, but also in simulation details, may cause this deviation. Furthermore, experimental demonstration of NaCl rejection using CVD graphene remains to be achieved as the only experimentally available result shows the peculiar case of negative rejection that may be related to the experimental procedure and data evaluation of that work.

In summary, liquid and ion transport across graphene has shown diverse behaviour in both theory and experiment that strongly varies with pore size, charge, and transporting solutes. The demonstration of selectively passing cations over anions paves the way for efficient reverse electrodialysis, and the demonstration of ion rejection is particularly important for the desalination

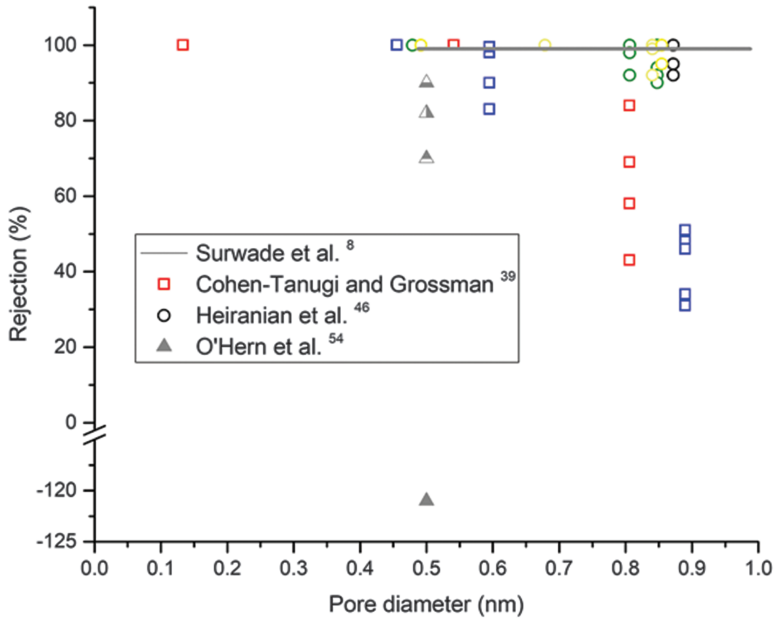


**Figure 3.3** NaCl rejection, unless specified differently, as a function of pore diameter. Inconsistent ion rejection at a given pore size needs further investigation. Symbols represent the corresponding study; colours represent chemical group at the pore edge. Red, blue, black, and grey represent hydrogen, hydroxyl, no, and unknown functionalization of graphene, respectively. Green, yellow and dark yellow represent Mo, S, or mixed pore edge atoms in $MoS_2$. Partially filled triangles represent $MgSO_4$, allura red, and dextran molecules.

applications. Substantial efforts are anticipated and required in obtaining selective molecular flow across graphene membranes at square centimetre or larger scales, which calls for a breakthrough in the manufacturing process. On the other hand, applications that require only a micrometre-scale membrane dimension, such as DNA sequencing or chem-bio sensing, might have more readiness for market entrance.

## 3.4 Proton and Atomic Species Transport Across Atomically Thin Membranes

Miao *et al.* used first principles DFT simulations to study atomic hydrogen and proton transport through pristine graphene.[56] Due to electron orbital overlap, repulsion forces are experienced by both hydrogen and protons. However, the energy barrier for passage of physisorbed hydrogen is 2.46 eV compared with physiosorbed protons experiencing only 1.41 eV. During passage, the graphene hexagons expand and contract again, reflecting the strong interaction, similar to gas molecules passing through nanopores.

This study demonstrates the principal possibility of hydrogen and proton passage through pristine graphene, however, the predicted energy barriers would be impractically high. The presence of defects such as double vacancies, on the other hand, significantly reduces the energy barrier for passage.

Experimentally, Hu *et al.* investigated the proton conductivity of mechanically exfoliated monocrystalline graphene, $MoS_2$, hBN, and multilayers of these materials with an applied electrical potential as the driving force.[57] By coating different 2D crystals with Nafion™ and measuring the current–voltage characteristics in a humid atmosphere, they found unexpectedly high transport through graphene and hBN monolayers, while single layer $MoS_2$ and bilayer graphene showed no transport. The variation in proton conductivity is rationalized by a variation in electron cloud density among the various materials as well as the difference between hBN and graphene in stacking behaviour, however, the fundamentals of the passage remain to be elucidated. Measuring proton conductivity at various temperatures allowed the passage energy barrier to be extracted, which was determined to be 0.78 eV and 0.3 eV for graphene and hBN monolayers, respectively. Platinum sputter coating of the 2D crystal further decreased the passage barrier, leading to immense proton conductivity for hBN. Further experiments of HCl conductivity measurements and mass spectroscopy verified the previously observed transport rates. The lower passage barrier compared with theoretical prediction requires further research.

Measuring aqueous proton transport across graphene in the absence of an external electric field as the driving force was reported by Achtyl *et al.*[58] Using alternating streams of acidic or basic solutions of the same strength flowing over a fused silica surface allowed them to probe the protonation and deprotonation of silanol at the silica surface by the second harmonic generation technique. The measured second harmonic time trace is indistinguishable for bare fused silica compared with fused silica covered by monolayer graphene from CVD, indicating unimpeded proton transport across the graphene layer. The same holds true for up to 8 layers of tested graphene. SEM analysis shows macroscopic defects of 500 nm and larger in diameter widely spread such that it is difficult to probe areas close to these defects due to the 30 μm wide laser spot. However, STEM analysis with atomic resolution reveals atomic scale defects to be always statistically present within the laser spot. DFT simulations and ReaxFF reactive force field MD simulations were performed to predict the aqueous proton transport mechanism across graphene. They obtained a 3.8 eV energy barrier for protons to pass through pristine graphene, which makes it an unlikely explanation of their results. However, for quad-vacancy atomic scale defects with various pore functionalization, they found that hydroxylated pores can allow proton passage with a moderate energy barrier of 0.6–0.7 eV as these can form hydrogen bonds with the adjacent water layers such that protons can shuttle across the defects in a Grotthuss mechanism at room temperature. Due to uncertainty of the atomic defect density estimation, the authors

state that other means of transport may yet be possible. Especially, the reason for indistinguishable traces for even eight layers of graphene remains elusive.

In the same year, a second study measured proton transport across CVD graphene by covering glass capillaries with single layer graphene and measuring current–voltage characteristics in the presence of a HCl concentration gradient.[59] Selective passage of protons over $Cl^-$ anions is observable by a measurable net current with no voltage applied. The reversal potential, the external potential required to stop the net current, allows the proton selectivity of the membrane to be extracted. While as-grown graphene shows only mild selectivity, depositing $Al_2O_3$ by ALD causes the total current across the graphene to decrease significantly, while at the same time, the reversal potential, and thus the selectivity, increases significantly. A reduction in total current and an increase in reversal potential after ALD coating is interpreted by the authors as proton transport through defects since the total current should be dependent on the defect size, which decreases with ALD coating, and increased selectivity could be caused by the reduction in defect size, such that they become more selective toward protons compared to $Cl^-$.

A theoretical analysis to resolve the discrepancy of the graphene tunnelling barrier between previous MD simulation and experiments was executed by Poltavsky *et al.*[60] They employed *ab initio* MD Feynman–Kac path-integral simulations that treat the atomic nuclei quantum-mechanically instead of classically. For comparison, they also carried out their simulation by treating the nuclei classically and they obtained similar transport barriers for the proton as earlier studies. The quantum mechanical treatment of the nuclei, however, predicts a significantly lower energy barrier for thermal protons to pass through graphene (0.6 eV) and this matched with that determined experimentally (0.8 eV) much better than the non-quantum-mechanical treatment of the nuclei. Thus, this theoretical study concludes favourably for the proton transport mechanism across pristine graphene.

Seel *et al.* investigated proton and atomic hydrogen transport across pristine 2D materials, such as graphene, hBN, $MoS_2$, and others by means of DFT to shed light on the question of proton transport through atomically thin 2D materials.[61] From their simulations, they found that system relaxation, that is, non-rigid 2D material atom positions, is a significant factor determining the penetration barrier height. Protons passing through graphene experience a 1.38 eV energy barrier, while hBN only poses a 0.11 eV energy barrier. Apart from slightly larger atomic bond lengths in hBN compared with graphene, the polarization of hBN is found to facilitate proton transport due to ionic bonding opportunities for protons arising during passage. Contrary to this result, $MoS_2$ is found to trap atomic hydrogen and protons in between the S-layers in a 1.56 eV deep energy well. They investigated the effect of Pt for passage without observing a different activation energy for passage. The presence of a quad-vacancy terminated by oxygen atoms reduces the passage barrier further to 1.1 eV, suggesting that

experimentally observed proton transport across graphene stems from defects, while hBN allows thermal proton passage.

Zhang *et al.* carried out ab-initio DFT calculations to better understand the differences in permeance of hydrogen isotopes, as previously demonstrated by Lozada-Hidalgo *et al.*[62,63] They compared graphene, hBN, alpha-boron, as well as graphene with Stone-Wales (55–77) defects. Pristine graphene is predicted to have a 1.5 eV passage barrier, while hBN only imposes a 1 eV barrier, both in quantitative opposition to experimentally measured values. However, the ratio of hydrogen isotope separation, *e.g.* proton/deuterium, based on differences in passage barrier and Arrhenius rate constants amounts to 12, close to the experimentally obtained values. The same holds true for proton/tritium separation with a predicted selectivity of 37, close to the experimentally measured value of 30. They further probed the passage barrier of Stone–Wales defects, where specifically proton transport across heptagons is found to experience a lower energy barrier of 0.55 eV and an increased proton/deuterium selectivity of 25, which is attributed to stronger interaction of protons with C–C bond connecting pentagons of the Stone-Wales defect. Furthermore, alpha-boron as a model system was investigated to yield a proton passage barrier of only 0.2 eV. The differences in passage barriers for 2D materials is attributed to the electron-density surfaces that reveal graphene, hBN, and alpha-boron to have different effective pore sizes experienced by a passing proton, resulting in the difference in the passage barriers.

Another study extended the analysis of proton permeation across two-dimensional materials from graphene and hBN to other materials such as phosphorene or silicene.[64] In their DFT simulations, they furthermore distinguished the proton permeation barrier depending on the environment around the membrane. Under vacuum, protons pass through graphene and hBN with 1.2 eV and 0.6 eV energy barriers for adsorption with subsequent passage. Changing the environment to aqueous solution is found to increase the proton penetration barriers to 3.3 eV and 3.0 eV for graphene and hBN, respectively, such that the authors concluded proton passage to be unlikely at room-temperature in an aqueous environment.

More efforts to understand and resolve the mismatch between theoretical and experimental proton permeation barriers across graphene and hBN were made by means of DFT simulation.[65] Structural optimization of the proton-2D-crytal arrangement was found to counterintuitively increase the permeation barrier. This could be explained by the previously unstable configuration of the proton in vacuum over the 2D crystal. System relaxation leads to proton adsorption to the respective crystal lattice such that the system is in a more stable state. Other effects of mechanical strain or curvature reduce the barrier by 0.1 eV or less and thus are unable to explain the discrepancy. Further simulations of a proton in aqueous phase also increased the permeation barrier to up to 5 eV for graphene, in qualitative agreement with the previous result[65] of a higher barrier to solvated protons in comparison to vacuum permeation.

In a study performed by Tsetseris *et al.*, DTF was applied to reveal details of the permeation process of atomic hydrogen, boron, nitrogen, and oxygen.[66] With passage energy barriers of 4.2 eV, 5.5 eV, and 3.2 eV for hydrogen, oxygen, and nitrogen, respectively, it was confirmed that pristine graphene can be considered impermeable also for these atomic species. Interestingly, the passage barrier for atomic boron is only 1.3 eV. In general, three passage ways for permeation of atomic species can be considered: direct passage through the centre of the hexagonal rings without C–C bond breaking, adsorption and passage involving breaking and reformation of C–C bonds, and more complex passages. Using minimum energy pathways, the authors determined all of the studied atomic species to predominantly undergo the second pathway involving breaking of C–C bonds by forming bonds with the passing atoms. Out of these, boron has a surprisingly low energy barrier, which may be overcome frequently at moderately high temperatures of around 200 °C.

Experimentally, selective hydrogen isotope transport was demonstrated by means of a Nafion™ coating of graphene or hBN monolayer in a 100% humidity atmosphere of either hydrogen–argon or deuterium–argon mixtures and then by performing current–voltage measurements and mass spectroscopy measurements.[63] The authors found a proton/deuterium selectivity of 10, which can be interpreted as a 60 meV difference in passage energy barrier. Interestingly, the selectivity is the same for graphene and for hBN, even though the total barriers differ. This result implies intrinsic differences between protons and deuterons to cause the observed selectivity. Indeed, the differences in zero-point energy of protons bound to oxygen of the $SO_3^-$ group of Nafion™ from those of deuterons matches the derived energy difference from the selectivity. This finding suggests the difference in zero-point energy is responsible for the experimentally observed selectivity. From the differences in zero-point energy, a proton/tritium separation factor of 30 is expected.

In a subsequent work, Lozada-Hidalgo *et al.* demonstrated the electrochemical pumping approach for CVD graphene on a one-inch scale with 95% macroscopic graphene coverage and a proton/deuteron separation factor of 8.[67] Since graphene works as an electrode of the electrochemical pump, these macroscopic pinholes are not expected to reduce the separation factor significantly, validating the utility of the technology. The energy requirements are less than the currently best available technological option showing the highest current selectivity and may be reduced further by using hBN and/or optimized operation conditions.

Despite these advances, the fundamental question about proton transport across pristine graphene persists, as can also be seen from Figure 3.4 showing the available results of energy barriers for protons to pass through graphene as a function of the number of missing carbon atoms from the lattice. An apparent mismatch between simulation and experiment can be observed. Particularly, the presence of atomic defects with a few atoms removed from the lattice are experimentally hard to rule out unambiguously.

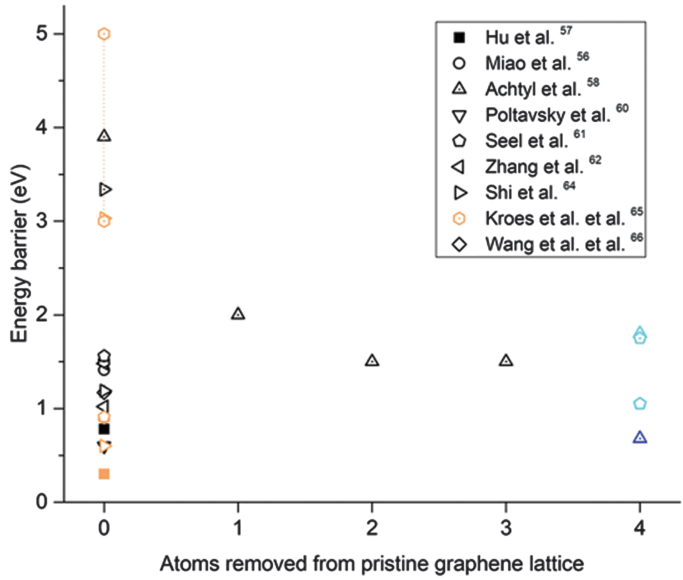


**Figure 3.4** Energy barriers for proton passage across graphene and hBN for various atoms removed from the lattice. The strong variation between available data for non-porous graphene transport barrier requires further study. Symbol shapes represent different studies. Filled and hollow symbols represent experimental and theoretical results, respectively, with black and brown representing graphene and hBN, respectively. Dotted symbols represent an aqueous environment. Blue and cyan represent graphene with hydroxyl and oxygen termination. Kroes *et al.* provided a range of penetration barriers in between the limits shown in the graph.[65]

## 3.5 Conclusion

Chemical species can transport across porous graphene or other two-dimensional membranes through various mechanisms depending on the phase and charge of each transporting species. Simulations and experiments agree that pristine graphene is generally impermeable to gases, while nanometre-scale pores punctured on graphene can provide transport pathways depending on the size relation, physicochemical interaction, and orientation of transporting molecules with pores, on the geometry and chemical functionalization state of the pore, and on the presence of non-permeating species. While the molecule-to-pore size ratio can primarily determine passage, a precise amount or rate of permeation of a gas species may be reliant on surface adsorption and diffusion or the chemical affinities of the species around the pore, factors often regarded as secondary effects to porous membranes. According to simulations, electron orbitals and the resulting electron probability density can effectively govern the interaction dimension between pore and molecule. From this finding, it is deduced that electron orbital overlap is strongly correlated with the energy barrier that

molecules face in an attempt of pore passage. For a certain pore size near 1 nm (slightly beyond the molecular sieving regime), adsorption to and surface diffusion on the membrane surface are likely to dominate the gas transport mechanism. This prediction may have significant implications for membranes in practice as a typical separation prediction based on molecular mass or kinetic diameter may not work for certain gas mixtures, possibly resulting in separation factors that belie those of molecular sieves, as exemplified by favourable permeation of unwanted species. Pores in the size regime tightly commensurate with the transporting molecular dimension are likely to separate a gas mixture *via* entropic gates that facilitate certain specifically oriented molecules. This approach may prove useful in the separation of gas species that are close in kinetic diameter but disparate in adsorption orientation. An idealization taken in many simulations is membrane rigidity, whose insignificant influence on separation has been put into question. In this light, experimental validation of predicted phenomena can be critical to clarify our molecular-level understanding of gas transport and separation across porous 2D materials. Similarly, no experiment to date has been able to reveal the disparity in separation correlated to functional groups at the pore edge and their charge state. For molecules of very similar kinetic diameters, the clear disparity in molecular interaction with pore functional moieties promises to allow meaningful separation of an almost inseparable mixture with conventional membranes, such as $N_2$ from $O_2$.

Experimentally, hermeticity and molecular-sieving-like large separation factors ($>10^4$ for a certain gas mixture) of mechanically exfoliated graphene have been established. Transport across exfoliated graphene with few pores is found to be time-variant, originating possibly from dynamic switching of the bond state of edge atoms of subnanometric pores. Flow physics of large-area CVD-grown graphene does not follow continuum-mechanics-based channel-flow models such as Hagen–Poiseuille flow but instead complies with Sampson's formula, a solution of a low-Reynolds-number flow across a 2D disc, where resistance to flow comes exclusively from a pore entry event. For the same reason, no Knudsen minimum in the permeance is observed at Knudsen numbers near unity. Regarding gas separation, a critical role of defects in graphene has been verified. Molecular sieving across defective graphene with subnanometric pores has been characterized in a single-gas permeance measurement followed by estimation of permselectivity. However, real applications demand sieving of gas mixtures, calling for methods to generate subnanometric defects in a facile, controllable, and scalable manner, while maintaining the ultimate permeance promise of graphene.

In order to apply the graphene- or 2D material based membranes to gas separation applications, there are a number of physical effects and technological aspects to account for. Demonstration of gas mixture sieving across CVD graphene membranes perforated with scalable processes needs to be achieved to move CVD graphene membranes from the laboratory to industry for applications such as air separation, $CO_2$ sequestration or other technologically relevant gas separations. Physical effects of charge and chemical

functionalization of a pore remain to be investigated, and the predicted blockage of non-permeating species in ternary mixtures defines both a scientifically interesting question – for the exploration of new means of separation – and a practically important task if considering a fact that most gas separation applications deal with complex mixtures beyond binary ones. Regarding system design, both ultrahigh selectivity and permeance of membranes may at some point add negligible performance improvement to an entire gas separation system owing to such external effects as concentration polarization, retentate recycling limitations, and so forth. With 2D membranes offering ultimate permeation, it may be possible to reach the technologically meaningful limit of permeance. Given a proper way of producing large membranes with subnanometric pores, the same may hold true for selectivity. Then, these membranes can be considered as the ultimate membranes, since further permeance or selectivity improvement of the membrane may not necessarily lead to deterministic system improvements; an ultimately permeable separation membrane is not the limiting factor anymore.

Regarding liquid transport, Sampson's formula governs the transport across a 2D aperture as long as continuum fluid can be assumed around the 2D aperture, although frequently, the Hagen–Poiseuille formalism is misused for subnanometric pores because both theories lead to comparable predictions for channels with pores of aspect ratio close to unity. Variation of permeance for different 2D materials such as $MoS_2$ has been theoretically predicted, though experimental confirmation is absent. Pore-sizes below the limit of continuum assumption have been predicted to exemplify subcontinuum variation in fluid properties such as density, viscosity or diffusivities for which experimental proof is still missing. Vapour transport studies across nanopores have so far been limited, however interesting questions about fluid properties during phase change and vapour interaction with graphene or other 2D materials can be thought of due to similar experimental observations in neighbouring fields.[68] The understanding of flow enhancement for CNT and nanofluidic channels may be broadened by considering transport across 2D nanopores that are at the limit of thinness and could present an idealized system of the former fields. Even though graphene has been proven as mechanically sturdy under applied pressure as simulation and previous mechanical characterization predicted, the question of how the mechanical properties will alter if graphene is perforated remains.[69,70] For use in practical applications, it will be necessary to probe the limits of mechanical strengths for various pore sizes, density and other membrane parameters, as has been predicted theoretically.[71]

Ionic transport has been investigated rather thoroughly and theoretically where the conductance of 2D nanopores decreases strongly at the continuum-limit, due to non-continuum effects such as variation in ion mobility, concentration, or dehydration barriers for passage. Nanopores with different functional groups exhibit a strong ion selective behaviour and a possible inter-co-ion selectivity depending on interaction strengths with

charged groups at the pore edge. For sufficiently small pores, desalination by reverse osmosis is predicted and experimentally shown using forward osmosis. Similar to pure liquid transport, distinct effects of the choice of 2D materials is predicted, although experimental proof is lacking. Experimentally shown, however, have been various ionic conductance phenomena of subnanometric pores such as Coulomb blockade or conductance similar to biological channels. At large pore sizes, linear scaling of conductance with pore diameter is most accurate due to the 2D geometry of the pore. This scaling is in line with the liquid transport where the transport rate shows a linear dependency on the pore size (*e.g.*, Sampson's formula), in contrast to three-dimensional descriptions. Besides, molecular sieving using centimetre-sized graphene and nanofiltration of charged species are established.

The effect of surface charge has been proposed as a significant means for selective ion transport even in pores much larger than a Debye screening length, raising the question of how to tailor the surface- and pore charge in order to engineer ionic transport for various pore sizes. Variation in surface charge by voltage gating may offer a pathway to achieve ion selectivity for pores larger than the hydrated diameters of the solutes to be rejected. For desalination applications, salt rejection by CVD-grown graphene perforated with scalable processes remains to be demonstrated in order to position graphene as a potential candidate for future desalination membranes. Proton transport as a special case of ionic transport due to differences in atomic configuration in solution has been experimentally shown and theoretically analysed, however the exact mechanism of transport remains disputed with some studies suggesting proton transport through pristine parts of graphene or hBN, while others suggest defects as the cause of the proton transport pathway. Here, more work is required to resolve the current issues and to enhance our understanding.

As an overarching goal, 2D membranes should be manufactured at length scales relevant to the respective application, which often involves square metres or even larger than that. To this end, synthesis and fabrication methods to yield nearly defect-free membranes need be established. One of the most important operational challenges in membrane separation processes is clogging and fouling of the membrane surface such that separation performance of the membrane deteriorates over time. 2D membranes might offer a unique advantage of reducing clogging and fouling exclusively to their surface compared with channel clogging and fouling in conventional membranes. Surface cleaning should be much less challenging, and thus 2D membranes may prove themselves to be practically beneficial for long lifetimes under chemically harsh conditions.

## Acknowledgements

We acknowledge the financial support from Commissions for Technology and Innovation (CTI), Federal Department of Economic Affairs, Education and Research (EAER), Switzerland (KTI-Nr. 18463.1 PFEN-MN). A part of this

work was financially supported by the Korea Institute of Energy Technology Evaluation and Planning (KETEP) and the Ministry of Trade, Industry, & Energy (MOTIE) of the Republic of Korea (No. 20168510011420) for which H.G.P. is grateful.

## References

1. H. B. Park, J. Kamcev, L. M. Robeson, M. Elimelech and B. D. Freeman, *Science*, 2017, **356**(6343), eaab0530.
2. R. W. Baker, *Membrane Technology,* John Wiley & Sons, Inc., 2012.
3. M. Elimelech and W. A. Phillip, *Science*, 2011, **333**(6043), 712.
4. B. Freeman and Y. Yampolskii, *Membrane Gas Separation,* John Wiley & Sons, Inc., 2011.
5. J. S. Bunch, S. S. Verbridge, J. S. Alden, A. M. van der Zande, J. M. Parpia, H. G. Craighead and P. L. McEuen, *Nano Lett.*, 2008, **8**(8), 2458.
6. M. D. Fischbein and M. Drndić, *Appl. Phys. Lett.*, 2008, 93(11), 113107.
7. K. Celebi, J. Buchheim, R. M. Wyss, A. Droudian, P. Gasser, I. Shorubalko, J. I. Kye, C. Lee and H. G. Park, *Science*, 2014, **344**(6181), 289.
8. S. P. Surwade, S. N. Smirnov, I. V. Vlassiouk, R. R. Unocic, G. M. Veith, S. Dai and S. M. Mahurin, *Nat. Nanotechnol.*, 2015, **10**(5), 459.
9. S. C. O'Hern, M. S. Boutilier, J. C. Idrobo, Y. Song, J. Kong, T. Laoui, M. Atieh and R. Karnik, *Nano Lett.*, 2014, **14**(3), 1234.
10. D. E. Jiang, V. R. Cooper and S. Dai, *Nano Lett.*, 2009, **9**(12), 4019.
11. Y. Li, Z. Zhou, P. Shen and Z. Chen, *Chem. Commun.*, 2010, **46**(21), 3672.
12. S. Blankenburg, M. Bieri, R. Fasel, K. Mullen, C. A. Pignedoli and D. Passerone, *Small*, 2010, **6**(20), 2266.
13. A. W. Hauser and P. Schwerdtfeger, *Phys. Chem. Chem. Phys.*, 2012, **14**(38), 13292.
14. H. Du, J. Li, J. Zhang, G. Su, X. Li and Y. Zhao, *J. Phys. Chem. C*, 2011, **115**(47), 23261.
15. J. Schrier, *ACS Appl. Mater. Interfaces*, 2011, **3**(11), 4451.
16. J. Schrier, *ACS Appl. Mater. Interfaces*, 2012, **4**(7), 3745.
17. L. W. Drahushuk and M. S. Strano, *Langmuir*, 2012, **28**(48), 16671.
18. C. Sun, M. S. Boutilier, H. Au, P. Poesio, B. Bai, R. Karnik and N. G. Hadjiconstantinou, *Langmuir*, 2014, **30**(2), 675.
19. M. Shan, Q. Xue, N. Jing, C. Ling, T. Zhang, Z. Yan and J. Zheng, *Nanoscale*, 2012, **4**(17), 5477.
20. K. Solvik, J. A. Weaver, A. M. Brockway and J. Schrier, *J. Phys. Chem. C*, 2013, **117**(33), 17050.
21. C. Z. Sun and B. F. Bai, *Sci. Bull.*, 2017, **62**(8), 554.
22. Y. Wang, Q. Y. Yang, C. L. Zhong and J. P. Li, *Appl. Surf. Sci.*, 2017, **407**, 532.
23. B. Wen, C. Sun and B. Bai, *Phys. Chem. Chem. Phys.*, 2015, **17**(36), 23619.

24. S. P. Koenig, L. Wang, J. Pellegrino and J. S. Bunch, *Nat. Nanotechnol.*, 2012, **7**(11), 728.
25. L. Wang, L. W. Drahushuk, L. Cantley, S. P. Koenig, X. Liu, J. Pellegrino, M. S. Strano and J. S. Bunch, *Nat. Nanotechnol.*, 2015, **10**(9), 785.
26. L. W. Drahushuk, L. Wang, S. P. Koenig, J. S. Bunch and M. S. Strano, *ACS Nano*, 2016, **10**(1), 786.
27. M. S. Boutilier, C. Z. Sun, S. C. O'Hern, H. Au, N. G. Hadjiconstantinou and R. Karnik, *ACS Nano*, 2014, **8**(1), 841.
28. M. S. Boutilier, N. G. Hadjiconstantinou and R. Karnik, *Nanotechnology*, 2017, **28**(18), 184003.
29. M. S. Boutilier, D. Jang, J. C. Idrobo, P. R. Kidambi, N. G. Hadjiconstantinou and R. Karnik, *ACS Nano*, 2017, **11**(6), 5726.
30. R. A. Sampson, *Philos. Trans. R. Soc., London A*, 1891, **182**, 449.
31. K.-K. Tio and S. S. Sadhal, *Appl. Sci. Res.*, 1994, **52**, 1.
32. R. Zan, Q. M. Ramasse, U. Bangert and K. S. Novoselov, *Nano Lett.*, 2012, **12**(8), 3936.
33. J. Lee, Z. Yang, W. Zhou, S. J. Pennycook, S. T. Pantelides and M. F. Chisholm, *Proc. Natl. Acad. Sci. U. S. A.*, 2014, **111**(21), 7522.
34. K. He, A. W. Robertson, C. Gong, C. S. Allen, Q. Xu, H. Zandbergen, J. C. Grossman, A. I. Kirkland and J. H. Warner, *Nanoscale*, 2015, **7**(27), 11602.
35. M. E. Suk and N. R. Aluru, *RSC Adv.*, 2013, **3**(24), 9365.
36. J. K. Holt, H. G. Park, Y. Wang, M. Stadermann, A. B. Artyukhin, C. P. Grigoropoulos, A. Noy and O. Bakajin, *Science*, 2006, **312**(5776), 1034.
37. I. Hanasaki and A. Nakatani, *J. Chem. Phys.*, 2006, **124**(14), 144708.
38. Z. Qin and M. J. Buehler, *Nano Lett.*, 2015, **15**(6), 3939.
39. D. Cohen-Tanugi and J. C. Grossman, *Nano Lett.*, 2012, **12**(7), 3602.
40. D. Cohen-Tanugi and J. C. Grossman, *J. Chem. Phys.*, 2014, **141**(7), 074704.
41. K. Sint, B. Wang and P. Král, *J. Am. Chem. Soc.*, 2008, **130**(49), 16448.
42. S. Zhao, J. Xue and W. Kang, *J. Chem. Phys.*, 2013, **139**(11), 114702.
43. M. E. Suk and N. R. Aluru, *J. Chem. Phys.*, 2014, **140**(8), 084707.
44. M. E. Suk and N. R. Aluru, *J. Phys. Chem. Lett.*, 2010, **1**(10), 1590.
45. Z. He, J. Zhou, X. Lu and B. Corry, *ACS Nano*, 2013, **7**(11), 10148.
46. M. Heiranian, A. B. Farimani and N. R. Aluru, *Nat. Commun.*, 2015, **6**, 8616.
47. S. Garaj, W. Hubbard, A. Reina, J. Kong, D. Branton and J. A. Golovchenko, *Nature*, 2010, **467**(7312), 190.
48. T. Jain, B. C. Rasera, R. J. Guerrero, M. S. Boutilier, S. C. O'Hern, J. C. Idrobo and R. Karnik, *Nat. Nanotechnol.*, 2015, **10**(12), 1053.
49. J. Feng, K. Liu, M. Graf, D. Dumcenco, A. Kis, M. Di Ventra and A. Radenovic, *Nat. Mater.*, 2016, **15**(8), 850.
50. J. Feng, M. Graf, K. Liu, D. Ovchinnikov, D. Dumcenco, M. Heiranian, V. Nandigana, N. R. Aluru, A. Kis and A. Radenovic, *Nature*, 2016, **536**(7615), 197.
51. A. Gadaleta, C. Sempere, S. Gravelle, A. Siria, R. Fulcrand, C. Ybert and L. Bocquet, *Phys. Fluids*, 2014, **26**(1), 012005.

52. R. C. Rollings, A. T. Kuan and J. A. Golovchenko, *Nat. Commun.*, 2016, **7**, 11408.
53. S. C. O'Hern, C. A. Stewart, M. S. Boutilier, J. C. Idrobo, S. Bhaviripudi, S. K. Das, J. Kong, T. Laoui, M. Atieh and R. Karnik, *ACS Nano*, 2012, **6**(11), 10130.
54. S. C. O'Hern, D. Jang, S. Bose, J. C. Idrobo, Y. Song, T. Laoui, J. Kong and R. Karnik, *Nano Lett.*, 2015, **15**(5), 3254.
55. P. R. Kidambi, R. A. Terry, L. Wang, M. S. H. Boutilier, D. Jang, J. Kong and R. Karnik, *Nanoscale*, 2017, **9**(24), 8496.
56. M. Miao, M. B. Nardelli, Q. Wang and Y. Liu, *Phys. Chem. Chem. Phys.*, 2013, **15**(38), 16132.
57. S. Hu, M. Lozada-Hidalgo, F. C. Wang, A. Mishchenko, F. Schedin, R. R. Nair, E. W. Hill, D. W. Boukhvalov, M. I. Katsnelson, R. A. Dryfe, I. V. Grigorieva, H. A. Wu and A. K. Geim, *Nature*, 2014, **516**(7530), 227.
58. J. L. Achtyl, R. R. Unocic, L. Xu, Y. Cai, M. Raju, W. Zhang, R. L. Sacci, I. V. Vlassiouk, P. F. Fulvio, P. Ganesh, D. J. Wesolowski, S. Dai, A. C. van Duin, M. Neurock and F. M. Geiger, *Nat. Commun.*, 2015, **6**, 6539.
59. M. I. Walker, P. Braeuninger-Weimer, R. S. Weatherup, S. Hofmann and U. F. Keyser, *Appl. Phys. Lett.*, 2015, **107**(21), 213104.
60. I. Poltavsky, L. Zheng, M. Mortazavi and A. Tkatchenko, *Arxiv*, 2016.
61. M. Seel and R. Pandey, *2D Mater.*, 2016, **3**(2), 025004.
62. Q. Zhang, M. Ju, L. Chen and X. C. Zeng, *J. Phys. Chem. Lett.*, 2016, **7**(17), 3395.
63. M. Lozada-Hidalgo, S. Hu, O. Marshall, A. Mishchenko, A. N. Grigorenko, R. A. Dryfe, B. Radha, I. V. Grigorieva and A. K. Geim, *Science*, 2016, **351**(6268), 68.
64. L. Shi, A. Xu, G. Chen and T. Zhao, *J. Phys. Chem. Lett.*, 2017, **8**(18), 4354.
65. J. M. Kroes, A. Fasolino and M. I. Katsnelson, *Phys. Chem. Chem. Phys.*, 2017, **19**(8), 5813.
66. L. Tsetseris and S. T. Pantelides, *Carbon*, 2014, **67**, 58.
67. M. Lozada-Hidalgo, S. Zhang, S. Hu, A. Esfandiar, I. V. Grigorieva and A. K. Geim, *Nat. Commun.*, 2017, **8**, 15251.
68. B. Radha, A. Esfandiar, F. C. Wang, A. P. Rooney, K. Gopinadhan, A. Keerthi, A. Mishchenko, A. Janardanan, P. Blake, L. Fumagalli, M. Lozada-Hidalgo, S. Garaj, S. J. Haigh, I. V. Grigorieva, H. A. Wu and A. K. Geim, *Nature*, 2016, **538**(7624), 222.
69. L. Wang, C. M. Williams, M. S. H. Boutilier, P. R. Kidambi and R. Karnik, *Nano Lett.*, 2017, **17**(5), 3081.
70. C. Lee, X. Wei, J. W. Kysar and J. Hone, *Science*, 2008, **321**(5887), 385.
71. D. Cohen-Tanugi and J. C. Grossman, *Nano Lett.*, 2014, **14**(11), 6171.